Journal of Power Sources 511 (2021) 230407

Contents lists available at ScienceDirect

Journal of Power Sources

journal homepage: www.elsevier.com/locate/jpowsour

Plasmon-enhanced dye-sensitized solar cells through porphyrin-silver nanoparticle hybrid structures: Experimental and computational studies

Rahim Ghadari [a,*], Alireza Sabri [a], Paria-Sadat Saei [a], Fantai Kong [b], Yousef Mohammadzadeh [a], Emre Guzel [c]

[a] Department of Organic and Biochemistry, Faculty of Chemistry, University of Tabriz, 5166616471, Tabriz, Iran
[b] Key Laboratory of Photovoltaic and Energy Conservation Materials, Institute of Applied Technology, Hefei Institutes of Physical Science, Chinese Academy of Sciences, Hefei, 230088, PR China
[c] Department of Engineering Fundamental Sciences, Faculty of Technology, Sakarya University of Applied Sciences, 54050, Sakarya, Turkey

HIGHLIGHTS

1. Ag NPs used to improve the efficiency of porphyrin-sensitized solar cells.
2. Ag@ZIF-8 core-shell NPs used to overcome the challenge of corrosion of Ag NPs.
3. The substituents of porphyrin alter the photovoltaic action of the solar cells.

ARTICLE INFO

Keywords:
Plasmonic effect
Dye-sensitized solar cells
Silver nanoparticles
Porphyrin

ABSTRACT

Surface plasmon resonance of silver nanoparticles (Ag NPs) was used to improve light absorption of porphyrins in plasmon-enhanced porphyrin-sensitized solar cells (PSSCs). Porphyrins with different substituents consisting –H, -Me, -MeO, –F, -Cl, -Br, $–CO_2H$, $–SO_3H$, $–NO_2$, and $–NH_2$ were used to study the effect of the interactions between photoactive dye molecules and plasmonic Ag NPs on the performance of PSSCs. The obtained results revealed that zinc tetra(4-carboxyphenyl)porphyrin and zinc tetra(4-aminophenyl)porphyrin have made the biggest impact on the performance of plasmon-enhanced PSSCs. Computational studies were done to study the electronic properties of porphyrin molecules with electron-withdrawing and electron-donating substituents interacted with Ag NPs. The theoretical studies confirmed that the electronic nature of substituents of porphyrins has a considerable effect on the electronic properties of porphyrin-AgNPs systems. In continue, Ag@ZIF-8 core-shell NPs were prepared to overcome the challenge of corrosion of Ag plasmonic nanoparticles. The results showed that using porphyrin-Ag@ZIF-8 systems, in many cases, the performance of PSSCs is increased relative to corresponding porphyrins but is decreased relative to porphyrin-AgNPs systems.

1. Introduction

Dye-sensitized solar cells (DSSCs) showed high power conversion efficiency (PCE) up to 14% [1]. By using abundant and non-toxic materials and the low cost of fabrication processes, they are attractive solar energy conversion technology [2–7]. Covering wide band gap semiconductors by the light harvester molecules in conjunction with electrolytes are all the components needed to achieve considerable solar-to-electric PCE using DSSCs [8–10]. By co-sensitization of wide band gap semiconductors by light harvester dyes it is possible to access noticeable absorption spectra of light [11]. In efficient co-sensitization of semiconductor by dye, some properties are essential for selected dyes; each dye could be able to be absorbed strongly on semiconductor surface and their molecules must be capable to transfer charge efficiently into the semiconductor. Their recombination must be low, and their regeneration can be done with the redox couple [12,13]. PCE of 15% will be accessible using I^-/I_3^- redox couple, if DSSCs can absorb about 80% of the light of solar spectrum from 350 to 900 nm [14,15]. The surface coverage as well as molar extinction coefficient of the sensitizing dye and the total surface area of the semiconductor film are determining keys for light absorption in DSSCs. The sensitizing dye has mostly been made from ruthenium-based complexes [16]. Although,

* Corresponding author.
E-mail address: r-ghadari@tabrizu.ac.ir (R. Ghadari).

https://doi.org/10.1016/j.jpowsour.2021.230407
Received 8 November 2019; Received in revised form 4 November 2020; Accepted 12 August 2021
Available online 1 September 2021

molar extinction coefficients of Ru-based dyes are generally low, but their absorption spectra are fairly broad. To address this issue, organic dyes with considerable molar extinction coefficients are developed recently [13]. Unfortunately, some organic dyes showed the narrow spectral bandwidths. Therefore, introducing new systems in which co-sensitization of semiconductor could considerably improve the efficiency of solar cells are important [17–21]. Light absorption is done by the dye molecules in DSSCs and the electron transport occurs in the nanostructured TiO_2. In DSSCs, the light absorption and charge transport do not take place in the same material; so, the absorption of light and collection of charge carriers may be affected in opposite ways by applying different changes in the solar device [22]. By changing dyes and employing light absorbers in DSSCs, light harvesting or carrier collection can be improved. Therefore, efforts to find more practicable approaches to improve the device performance without altering other properties of DSSCs has been continued [3]. Recently, surface plasmon resonance (SPR) of metal nanoparticles (MNPs) has showed unique capability to improve light absorption in semiconductor nanostructure-based light-harvesting assemblies of DSSCs with minimal effect on other efficiency factors of device [23–29].

Plasmons in metallic structures (known as plasmonics) are the collective oscillations of free electrons as the result of their response to incident waves [30–32]. It is reported that the coupling of plasmonic nanoparticles (PNPs) with semiconductor nanostructures of DSSCs would change the photovoltaic behaviors of light-harvesting assemblies [27,29,33,34]. Studies showed that the role of PNPs in plasmon-enhanced DSSCs are based on various possible reasons; for example, improved light absorption of PNPs as a result of their light-trapping effects, effective charge separation due to localized electromagnetic field of PNPs, improved electron transfer to the adsorbed species, and the effects of electron storage to drive the Fermi level to more negative potentials [23,35]. Since the marriage between semiconductor and PNPs in which PNPs is contacted directly with the dye and the electrolyte, recombination of photogenerated carriers and corrosion of PNPs by electrolytes is occurred, core-shell nanostructures of PNPs have been applied to address these issues [36,37]. In this work, we combine the use of porphyrins and silver nanostructures and the effect of plasmonic nanoparticles, to study the light harvesting of dyes in conjunction with plasmonic nanoparticles in porphyrin-sensitized solar cells (PSSCs). In continue, Ag@ZIF-8 core-shell NPs were prepared using the shell of ZIF-8, a type of zinc-based zeolitic imidazolate framework to overcome the challenge of recombination of photogenerated carriers and corrosion of PNPs. Also, ZIF-8, as highly porous MOF, can act as the scattering layers of photoanodes in PSSCs and prevent the penetration of light beyond the photoanode to increase the efficiency of the prepared cell.

2. Experimental methods

2.1. Materials

Pyrrole (C_4H_5N, ≥97.0%), the required benzaldehyde derivatives (benzaldehyde (C_7H_6O, ≥99.0%), 4-methylbenzaldehyde (C_8H_8O, ≥97.0%), 4-methoxybenzaldehyde ($C_8H_8O_2$, ≥98.0%), 4-fluorobenzaldehyde (C_7H_5FO, ≥98.0%), 4-chlorobenzaldehyde (C_7H_5ClO, ≥98.0%), 4-bromobenzaldehyde (C_7H_5BrO, ≥98.0%), 4-nitrobenzaldehyde ($C_7H_5NO_3$, ≥98.0%), and terephthalaldehydic acid ($C_8H_6O_3$, ≥98.0%)), terpineol ($C_{10}H_{18}O$, ≥80.0%), zinc acetate dihydrate ($C_4H_6O_4Zn.2H_2O$, ≥99.0%), sodium hydroxide (NaOH, ≥97.0%), sodium hydrogen carbonate ($NaHCO_3$, ≥99.5%), and tetrapropyl orthotitanat ($C_{12}H_{28}O_4Ti$, ≥ 98.0%) were purchased from Merck. Ethyl cellulose was purchased from Aldrich. All solvents (propionic acid, acetic acid, methanol, ethanol, acetone, acetic anhydride, chloroform, acetonitrile, and *tert*-butanol), concentrated HCl, concentrated sulfuric acid, and concentrated NH_4OH were obtained from Aldrich or Merck and used without further purification. FTO substrates, Pt paste, and standard iodine based electrolyte were obtained from Sharif-Solar (IRASOL). Surlyn was purchased from SUNLAB. Titanium oxide nanopowder (TiO_2, anatase, 99+%, 10–25 nm) was obtained from US Research Nanomaterials, Inc.

2.2. Synthesis and characterization of meso-tetraphenylporphyrin derivatives (H_2TXPP) and zinc meso-tetraphenylporphyrin derivatives (ZnTXPP)

The porphyrins H_2TPP, H_2T(Me)PP, H_2T(MeO)PP, H_2T(F)PP, H_2T(Cl)PP, H_2T(Br)PP, and H_2TCPP were prepared by the methods described in the literature (Scheme 1) [38–40]. Briefly, propionic acid (30 mL) was brought to boil and the corresponding benzaldehyde (4.0 mmol) was added. In continue, a fresh solution of pyrrole (4.0 mmol) in propionic acid (10 mL) was added to the prepared solution, dropwise. The mixture was refluxed for 1.5 h. After cooling to r.t., it was crystallized in the refrigerator overnight. The resulted product was filtrated and then the black solid residue was washed with hot water and methanol several times. Using Soxhlet methanol extraction, the purified H_2TXPP was obtained. Then, it was dried at r.t.

H_2TSPP was synthesized using H_2TPP by previously reported methods (Scheme 1) [41,42]. Briefly, H_2TPP (3.25 mmol) was added to the 20 mL of concentrated sulfuric acid and grounded together until a homogenous paste was obtained. After the addition of 50 mL of conc. H_2SO_4, the mixture was heated at 110 °C for 4 h and then allowed to stand at r.t. for 48 h. The prepared solution was filtered and the resulted filtrate was diluted carefully by the addition of distilled water. The obtained bright green precipitate was further purified by methanolic ammonia and acetone.

The preparation of H_2TNPP and H_2TAPP is done based on the reported method (Scheme 1) [43]. *p*-nitrobenzaldehyde (73.0 mmol) was added to the stirring solution of acetic anhydride (12.0 mL) in propionic acid (300 mL). The resulting solution was brought to reflux. Then, a fresh solution of distilled pyrrole (73.0 mmol) in propionic acid (10.0 mL) was added. The stirring mixture was refluxed for 30 min. The reaction mixture was allowed to cool and stand for 24 h in the refrigerator. After filtration, the dark solid was washed with distilled water and dried at r.t. Finally, the black produced powder was added to the stirring solution of pyridine (80.0 mL) and refluxed for 1 h. The reaction mixture was cooled to r.t. and then stored in the refrigerator overnight. The mixture was filtered and the residual solid was washed repeatedly with acetone to obtain pure H_2TNPP. H_2TAPP was synthesized using the reduction of H_2TNPP as a starting material. For this purpose, a solution of H_2TNPP (2.50 mmol) in concentrated HC1 (100 mL) was prepared under the bubbling of Ar for 1 h. A solution of $SnC1_2.2H_2O$ (40.0 mmol) in concentrated HC1 (15 mL), which was bubbled with Ar, was added to the prepared solution. The final mixture was heated (water bath, 80 °C) under stirring for 30 min. The hot-water bath was carefully replaced by a cold-water bath and then an ice bath. Neutralization of the solution was done under Ar by the slow addition of concentrated NH_4OH. The crude product was filtered and the greenish solid residual was stirred vigorously with a solution of NaOH (5%). After filtration, the H_2TAPP was washed with H_2O, dried. At the end, Soxhlet extraction with chloroform was performed to obtain pure H_2TAPP.

Metalloporphyrins ZnTPP, ZnT(Me)PP, ZnT(MeO)PP, ZnT(F)PP, ZnT(Cl)PP, ZnT(Br)PP, ZnTSPP, ZnTNPP, and ZnTAPP were synthesized by the previously described approaches (Scheme 1) [39,44,45]. In brief, ZnTXPP was prepared by the reaction of H_2TXPP (1.0 equivalent) with zinc(II) acetate dihydrate (1.2 equivalent) in methanol for 3–4 h. Finally, metalloporphyrins were filtered, washed, and dried at r.t. In the case of ZnTCPP synthesis [46,47], after filtration the product of reaction consisting of H_2TCPP and 1.2 eq of $Zn(OAc)_2.2H_2O$, the crude product was washed with methanol and dried, and then was dissolved in the aqueous solution of sodium bicarbonate (1.0 M). ZnTCPP product was precipitated with dropwise addition of a 1.0 M acetic acid solution. After filtration, the final product was washed with distilled water and

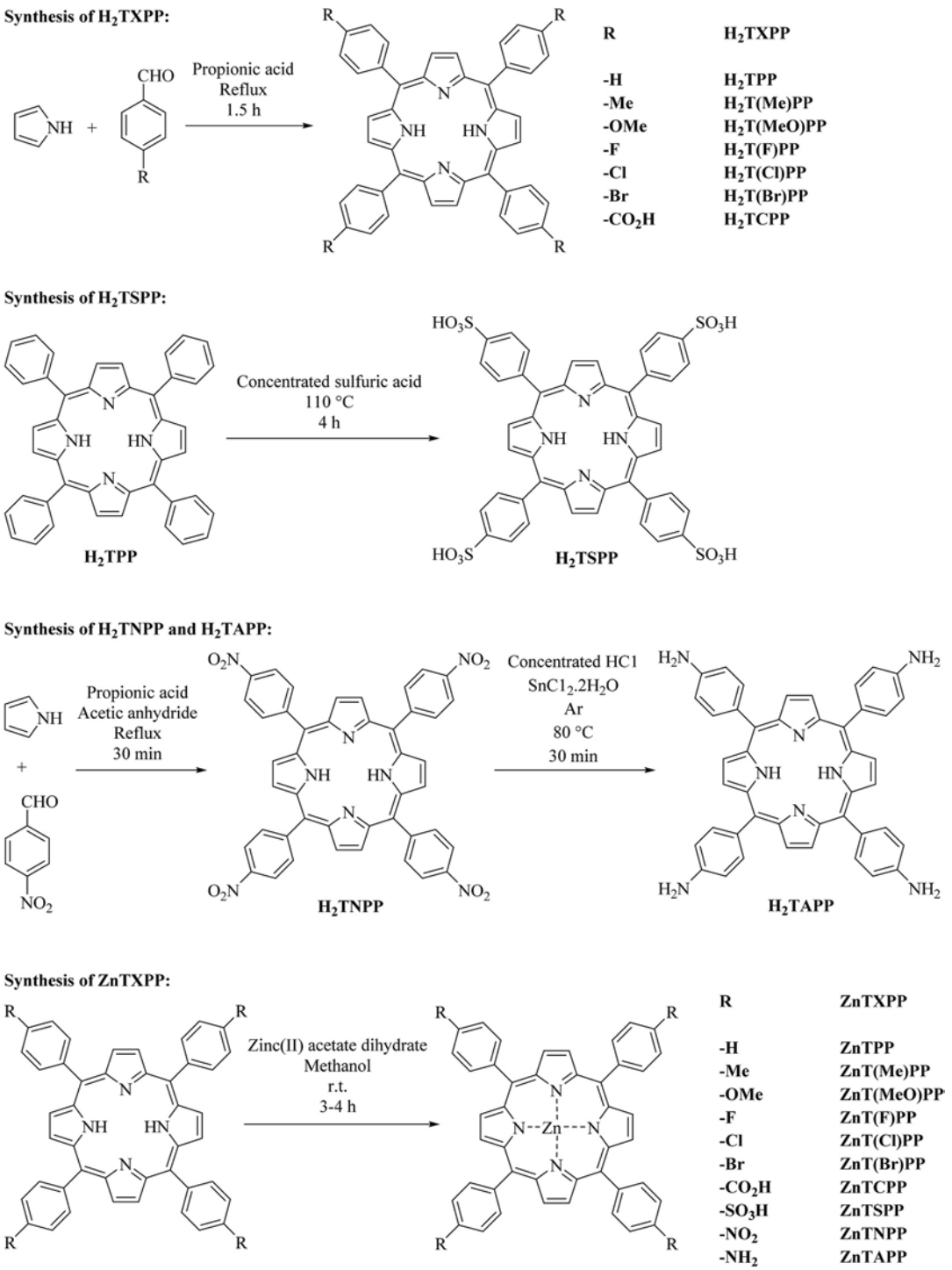

Scheme 1. Synthesis of H_2TXPP and ZnTXPP derivatives.

methanol and dried at r.t.

The NMR and UV–Vis data related to the synthesized porphyrins are provided in the electronic supplementary information (ESI).

2.3. Hybrid nanostructure synthesis

The procedure described by Murphy et al. was used to prepare AgNPs and ZnTXPP-AgNPs hybrid nanostructures [48]. In brief, to the solution of silver nitrate in deionized (DI) water (125 mL, 1 mM), a solution of sodium citrate (5 mL, 47 mM) and citric acid (5 mL, 52 mM) in DI water was added with vigorous stirring. The vigorous stirring is continued for 15 min, then, the dropwise addition of sodium borohydride solution (0.9 mL, 130 mM) in DI water was done. ZnTXPP-AgNPs was prepared by mixing an ethanolic solution of ZnTXPP with Ag nanoparticles in water. For this purpose, ZnTXPP powder was dissolved in ethanol, sonicated for 30 min, and stirred for 4 h to prepare an ethanolic solution. Finally, hybrid nanostructures were prepared using the mixing of the prepared ethanolic media by an aqueous suspension of Ag NPs.

To prepare the Ag@ZIF-8 core-shell system the previously reported method was used [49,50]. In brief, three solutions including the Ag NPs (0.16 mg mL^{-1}, 500 mL), $Zn(NO_3)_2.6H_2O$ (0.278 M, 10 mL), and 2-methylimidazole (0.556 M, 10 mL) were prepared. MeOH was used as

the media. The three prepared solutions were mixed and the reaction media was magnetically stirred for 3 h by keeping the temperature at 15 °C. After that, the reaction media was left a side without stirring to give enough time for the growth of the ZIF-8 on the surface of the Ag NPs. The obtained Ag@ZIF-8 NPs were separated by using centrifugation. The obtained NPs were washed by MeOH four times and then dried. To prepare the ZnTXPP-Ag@ZIF-8, the solution of the ZnTXPP and Ag@ZIF-8 NPs in the EtOH were mixed. The stirring of the mentioned mixture was resulted the ZnTXPP-Ag@ZIF-8.

2.4. Pastes and photoanode preparation

The photoanode was fabricated by previously reported procedures [51–54]. The transparent TiO_2 paste consisting a mixture of TiO_2 NPs (20 nm), ethyl cellulose, terpinol, and acetic acid in ethanol was prepared and followed by stirring and sonicating. The reflector TiO_2 paste was prepared with the same method using 300 nm TiO_2 NPs. Fluorinated tin oxide (FTO)-on-glass substrates (15 Ω/cm^2) were cleaned by washing with detergent and sonicating in DI water, HCl (0.1 M), acetone, and ethanol for 20 min, respectively. The FTO glasses were dried under flowing N_2 gas. The cleaned FTO substrates were soaked into titanium isopropoxide (Ti(i-pro)$_4$, 40 mM) solution at 50 °C for 30 min to form a compact TiO_2 layer. After that, the substrates were rinsed with DI water and ethanol and dried. After the preparation of viscous white TiO_2 pastes, the transparent paste and reflector paste were printed onto the Ti(i-pro)$_4$-treated FTO glasses by the doctor-blading method, respectively. The prepared anode was gradually heated in a muffle furnace under air flow at 125 °C (15 min), 325 °C (5 min), 375 °C (5 min), 450 °C (15 min), and 500 °C (30 min) to the TiO_2 layers be annealed. The annealed TiO_2 layers were once again treated with 40 mM Ti(i-pro)$_4$ solution at 50 °C for 30 min, as previously described. The prepared anode was rinsed with DI water and methanol and sintered at 500 °C for 30 min in a muffle furnace. After cooling to 80 °C, the prepared photoanode was immersed into 0.5 mM dye solution in a mixture of acetonitrile/*tert*-butanol (volume ratio, 1:1) and kept at room temperature for 16 h. Washing the photoanode with acetonitrile was done to remove the physically-adsorbed dye molecules.

2.5. Fabrication of DSSCs

To prepare the Pt counter electrode, FTO substrate with drilled holes, was washed with the same method as used for the working electrode. The Pt paste was printed onto cleaned FTO-glass by doctor blade method. The prepared paste was annealed at 460 °C for 15 min in a muffle furnace under atmosphere. For fabricating DSSCs, the dye-adsorbed TiO_2 electrode and counter electrode were assembled into a sandwich-type cell using a 50 μm thick thermoplastic spacer (Surlyn) with an open area of 0.25 cm^2. The photoanode was sealed to counter electrode by heating at 120 °C for about 90 s. An acetonitrile solvent-based electrolyte, composed of 0.05 M iodine, 0.1 M lithium iodide, 0.6 M 1,2-dimethyl-3-propylimidazolium iodide, and 0.5 M 4-*tert*-butylpyridine, was injected into the cell and sealed with a piece of the Surlyn spacer (Fig. 1).

2.6. Characterization

The optical absorption characteristics of the plasmonic NPs, the synthesized dyes, and hybrid nanostructures were evaluated using a Shimadzu UV-2100 spectrophotometer. Scanning electron microscopy (SEM) observations were carried out on a scanning electron microscope (TESCAN Vega Model). All samples were sputtered with gold before observation. Transmission electron microscopy (TEM) characterization was performed using LEO 906 transmission electron microscope (Zeiss, Germany) at 100 kV acceleration voltage. X-ray photoelectron spectroscopy (XPS) analysis was carried out using Thermo Fisher Kalpha instrument with Al Kα Monochromatic (1486.68 eV). Impedance studies were carried out using IviumStat instrument. NMR spectra were recorded on a Bruker Spectrospin Avance 400 spectrometer 400 MHz; chemical shifts are reported in parts per million (ppm).

Photovoltaic measurements were performed under illumination generated by an AM 1.5 solar simulator (Fan Daghigh Kosar, SIM2002) with a 300 W xenon lamp and an air-mass 1.5 global filter. The power of

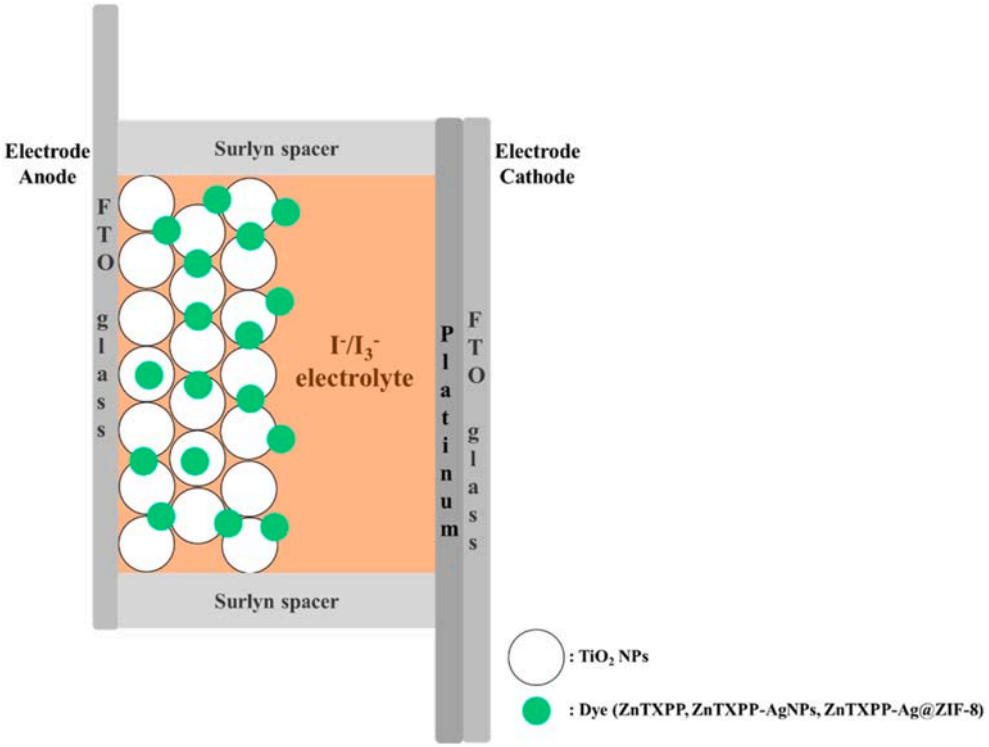

Fig. 1. Schematic representation of PSSCs.

the simulated light was calibrated to 100 mW/cm^2 (1 SUN) by using a reference silicon solar cell. The J-V curves were obtained by applying an external bias to the cell and measuring the generated photocurrent with a Fan Daghigh Kosar model IV2000 digital source meter. The voltage step and delay time of the photocurrent were 15 mV and 1 s, respectively.

3. Results and discussion

To prepare Ag NPs, to the vigorously stirring solution of $AgNO_3$, sodium citrate, and citric acid in DI water, an aqueous solution of $NaBH_4$ was added dropwise. Growth of the plasmon peak was monitored by UV–Vis absorption spectrophotometry and obtained data are presented in Fig. 2-a. The wavelength of the maximum absorption around 400–500 nm is attributed to the surface plasmon resonance of Ag NPs [55,56]. The addition of $NaBH_4$ is continued until the plasmon peak stopped growing, in which a complete reduction of silver ions occurs.

The SEM micrograph of the prepared Ag NPs is shown in Fig. 2-b. In SEM micrograph, spherical nanoparticles are observable in the size range of 20–30 nm. The size of these nanoparticles deduced from SEM is in agreement with the one measured by TEM (Fig. 2-c) that indicates a distribution of Ag nanoparticle sizes ~10–25 nm in diameter. It has been previously reported that the heterogeneous mixture of shapes and sizes are the result of sodium citrate usage in Ag NPs synthesis [48,57–60]. DLS was used to determine the size distribution of synthesized silver NPs (Fig. 2-d,e). The size distribution histogram of DLS indicated that the average size of the synthesized Ag NPs is 25.5 nm.

SEM observations of Ag@ZIF-8 NPs display that the diameter of the product is about 120 nm with similar shape (Fig. 3-a). Fig. 3-b is the TEM image of Ag@ZIF-8 NPs that is showing the ZIF-8 shell layer covering Ag NPs which is essential for the protection of the plasmonic Ag core from corrosion by the electrolyte during solar cell operation. Also, the size distribution histogram of DLS showed a relatively wide size distribution of particles (Fig. 3-c,d) that confirmed the obtained results of SEM analysis.

The energy-dispersive X-ray (EDS) elemental mapping of the prepared Ag@ZIF-8 NPs discloses that the element Ag and the elements C, N, and Zn attributed to ZIF-8 are homogeneously distributed in the prepared system. The result of the DES analysis is presented in Fig. S1 (electronic supplementary information (ESI)) that the obtained results confirmed the presence of the consisting elements C, N, Zn, and Ag in the prepared Ag@ZIF-8 NPs.

To ensure the presence of the elemental Ag as Ag@ZIF-8, XPS study was carried out. The results are presented in Fig. 4. In this figure, the binding energies of the elements are provided. Based on the obtained results the presence of the C, N, Zn, and Ag can be confirmed. Also, the absence of the other peaks is showing the purity of the prepared compound. From Fig. 4-b, the binding energy of the Ag 3d5/2 and Ag 3d3/2 were found to be 368.1 and 374.1 eV. These two peaks are because of the Ag 3d of Ag@ZIF-8 [61]. The mentioned peaks can be used to confirm the presence of the zero valence Ag NPs that were encapsulated by ZIF-8. Also, the observation of the mentioned peaks can confirm the stabilizing of the Ag NPS from oxidation by ZIF-8. The binding energies equal to the 399.1 and 386.1 eV are related to the N 1s and C 1s, respectively. The peaks at the 1022.1 and 1045.1 eV are related to the Zn 2p3/2 and Zn 2p1/2, respectively [61].

To better understand the influence of substituents on electronic structures of the frontier orbitals and explore the electronic characteristic on the performance of porphyrins and the prepared devices, density functional theory (DFT) calculation was carried out based on (U)B3LYP/6-311G(d) basis set using Gaussian 09 (Rev. A.01) program. In the case of the Ag containing calculations, the 6-311G(d) basis set for all atoms other than Ag was used. For Ag atom, LANL2DZ basis set was used. The calculated HOMO and LUMO orbitals of porphyrins employing DFT calculations are presented in Fig. S2 (ESI), in which all the LUMOs of H_2TXPP and ZnTXPP porphyrins delocalized mostly over the porphyrin ring. Also, for H_2TXPP and ZnTXPP porphyrins, the HOMO delocalized mainly on the central ring of porphyrins. In all of the presented HOMO and LUMO orbitals, positive and negative lobes are showed by orange and purple colors. As it is presented in Fig. S2 (ESI), electron distributions in the frontier orbitals of all of the H_2TXPP and ZnTXPP porphyrins are mostly over the porphyrin ring due to the perpendicular position of phenyl rings to the porphyrin ring, in which it is not be able to contribute in electron distributions [62]. It is well known that the dyes consisting anchoring group with electron density distribution of LUMO have different electronic behavior rather than those that have anchoring group which do not participate in electron conjugation when the excited adsorbed dye is coupled to TiO_2 NPs [62]. The energy levels of frontier orbitals and the main excitation properties for the H_2TXPP and ZnTXPP porphyrins are shown in Table 1. As it is presented in Table 1, there are one main electronic transitions in the visible region for all of the H_2TXPP porphyrins. Also, two main electronic transitions in the visible region are observable for all of the ZnTXPP porphyrins.

The energy levels of frontier orbitals and the main excitation properties for the ZnTXPP-AgNPs (Fig. S3) are listing in Table 2.

Substituted porphyrins with various kind of electron withdrawing and electron donating substituents with inductive and resonance effects were selected and prepared to study the role of hybrid molecular-plasmonic nanostructures in the performance of DSSCs. Because of the strong coupling of surface plasmons of PNPs to the molecular electronic transitions of the photoactive molecules, hybrid molecular-plasmon states will be created in the metallic nanoparticle-photoactive molecule systems [48]. Also, the localized surface plasmon resonance (LSPR) can interact with the excited states of the molecules in the hybrid molecular-plasmonic nanostructures. The mentioned interactions lead to change in the photonic properties. The overall result is an improvement in charge and energy transfer. Strong coupling of the photoactive molecules with surface plasmon of PNPs can be seen in systems in which the absorption of the molecule is near to the frequency of the LSPR. Due to the strong absorption of porphyrin molecules in the visible range, porphyrins are capable to overlap significantly with the plasmon band of Ag NPs. It was previously reported that porphyrins coupled to metallic nanostructures could show charge transfer and plasmon-enhanced electrical conduction [48]. As mentioned previously, incident light creates LSPR in metallic NPs *via* excitation of coherent oscillation of the free electrons. To study the interaction of photoactive porphyrin molecules with silver metallic nanostructures, the absorption spectra for ZnTXPP in the presence and absence of Ag NPs were examined. The obtained data are presented in Fig. S4 (ESI).

The role of substituents of the prepared ZnTXPP in interaction with Ag NPs was investigated to find the best dyes to be used as sensitizer in DSSCs. The prepared porphyrins were chosen for comparison based on the electronic character of their functional groups. For this purpose, various kinds of electron acceptor and electron donor substituents competing for inductive and resonance effects in the substituted porphyrin were selected and prepared. Therefore, absorption spectra of ZnTPP, ZnT(Me)PP, ZnT(MeO)PP, ZnT(F)PP, ZnT(Cl)PP, ZnT(Br)PP, ZnTCPP, ZnTSPP, ZnTNPP, and ZnTAPP, and all of them with the same concentration of Ag NPs are studied and their results are presented in Fig. S4 (ESI). Nitro, carboxyl, and sulfonic acid substituents in ZnTNPP, ZnTCPP, and ZnTSPP are electron withdrawing groups with resonance. It is leading to make rings to be electron poor relative to ZnTPP. The amino and methoxy groups have electron-donating nature *via* resonance. Alkyl substituents are electron-donating groups due to weak resonance effects come from σ-conjugation (hyperconjugation), so the porphyrin ring in ZnT(Me)PP is more electron rich than that of ZnTPP. In ZnT(F)PP, ZnT(Cl)PP, and ZnT(Br)PP porphyrins; the halogen substituents are electron withdrawing by inductive effect. It makes the porphyrins ring more electron deficient than that of ZnTPP. Also, the halo substituents through their electron donating resonance effect, lead the porphyrin ring of ZnT(F)PP, ZnT(Cl)PP, and ZnT(Br)PP to have a lower ability to interact with Ag NPs. Because of the slightly electron

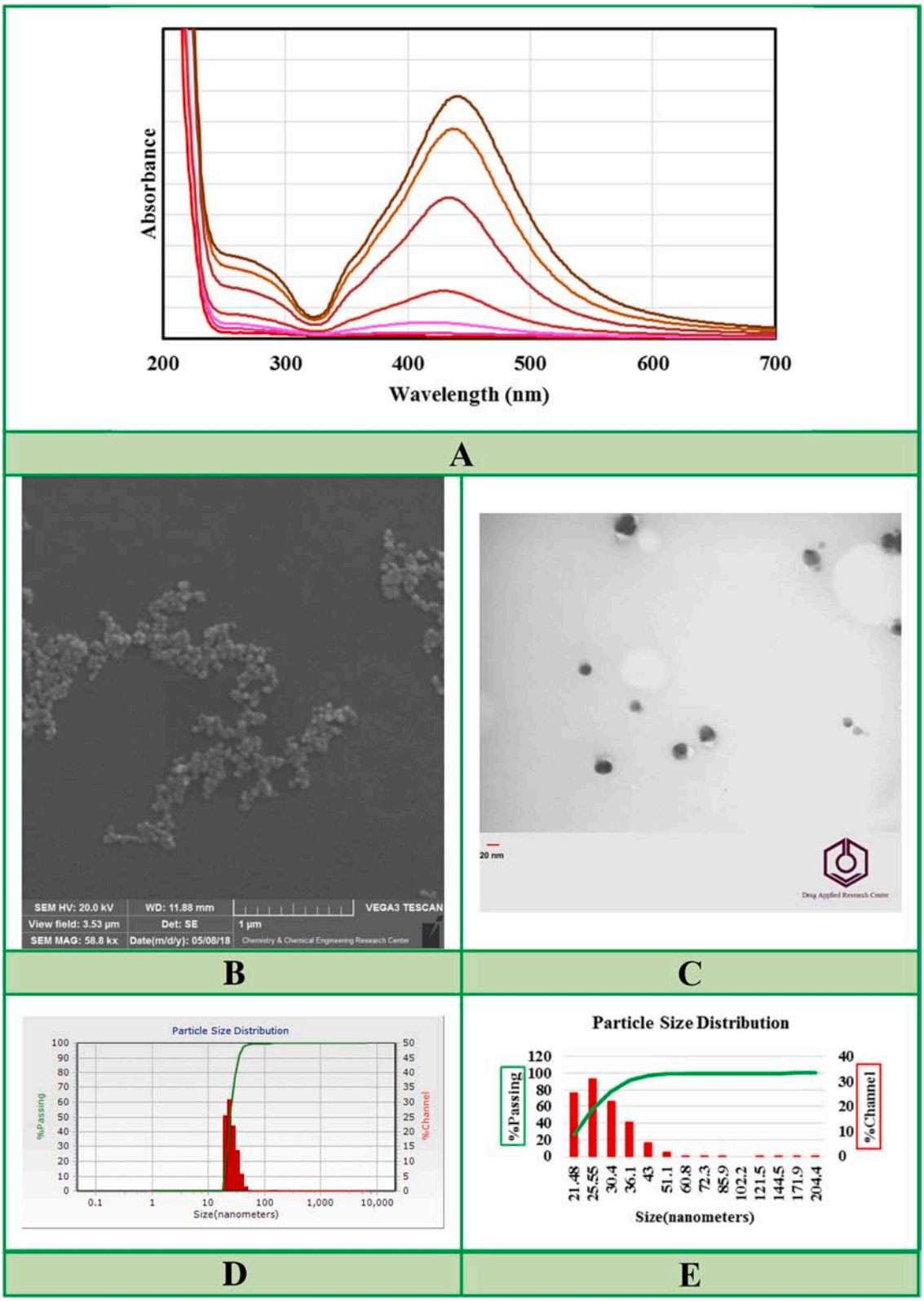

Fig. 2. UV–Vis absorption spectra of AgNPs showing the SPR peak from 410 to 440 nm (a), SEM (b) and TEM images of the prepared Ag nanoparticles (c), and size distribution of Ag NPs measured by the DLS technique (d, e); the %channel is showing the percentage of particles with the size presented at the horizontal axis, the % passing is showing the amount of the particles that are smaller than the size that is presented in the horizontal axis.

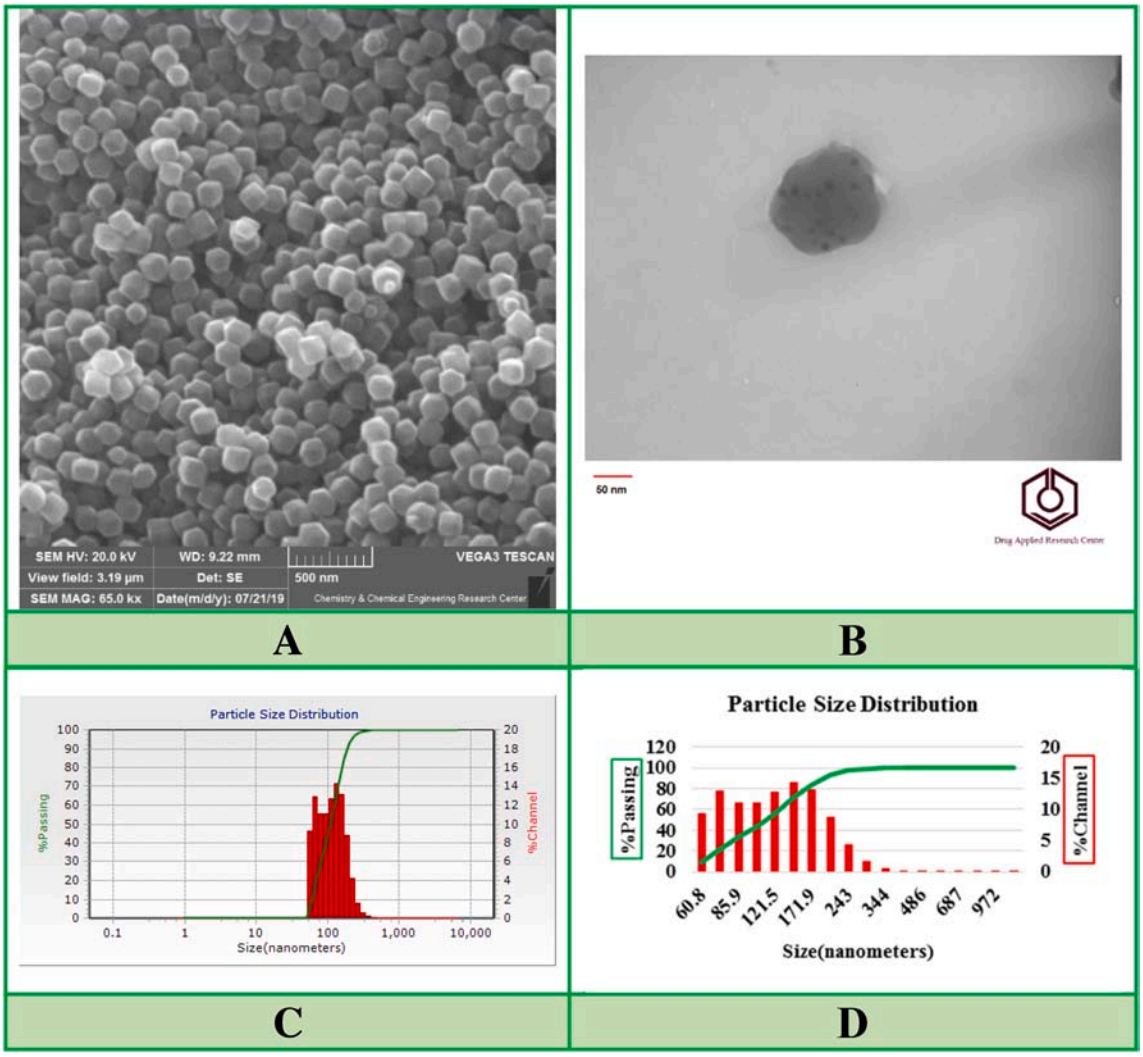

Fig. 3. SEM (a) and TEM (b) images of the prepared Ag@ZIF-8 NPs and size distribution of Ag@ZIF-8 NPs measured by the DLS technique (c, d).

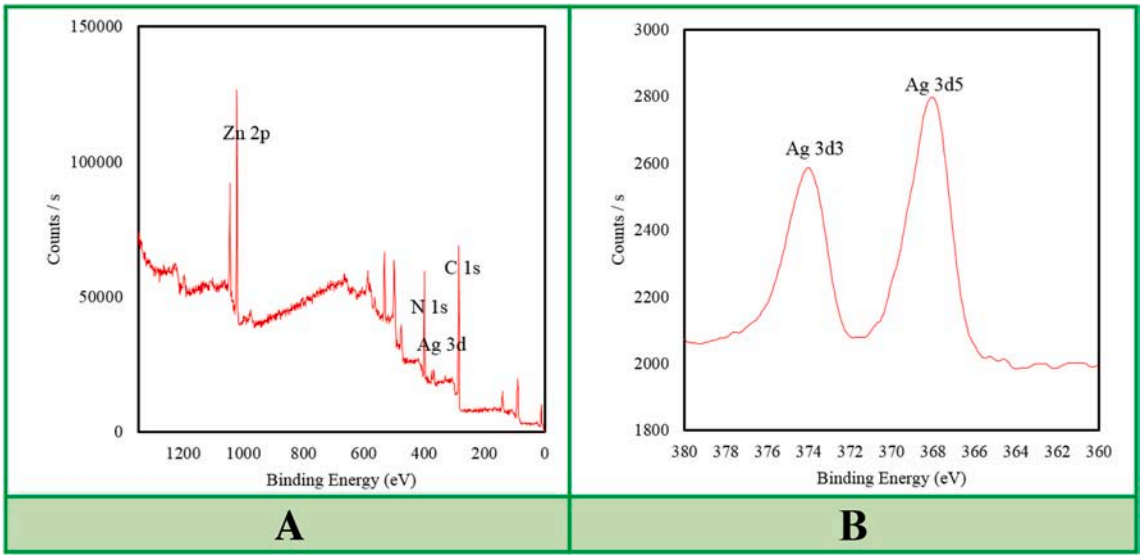

Fig. 4. XPS spectra of the prepared Ag@ZIF-8 NPs: XPS survey spectrum (a) and binding energy spectrum for Ag 3d (b).

Table 1
The energy levels of frontier orbitals and the main excitation properties for the H_2TXPP and ZnTXPP porphyrins. HOMO/LUMO energy unit: eV. The (U)B3LYP/6-311G(d) level of theory is used to perform both structure optimization and time-dependent density-functional theory (TD-DFT) calculations.

Dye	HOMO	LUMO	Wavelength (nm)	f (oscillating strength)	Orbitals
H_2TXPP					
H_2TPP	−5.20	−2.43	376.93	1.2672	HOMO-1 → LUMO
H_2T(Me)PP	−5.10	−2.35	378.91	1.3697	HOMO-1 → LUMO
H_2T(MeO)PP	−5.01	−2.29	388.51	1.0595	HOMO-1 → LUMO+1
H_2TFPP	−5.46	−2.68	377.35	1.2431	HOMO-1 → LUMO
H_2T(Cl)PP	−5.57	−2.79	378.32	1.3510	HOMO-1 → LUMO+1
H_2T(Br)PP	−5.56	−2.79	378.84	1.3936	HOMO-1 → LUMO+1
H_2TCPP	−5.57	−2.82	385.15	1.2977	HOMO-1 → LUMO+1
H_2TSPP	−5.94	−3.19	384.97	1.3511	HOMO-1 → LUMO+1
H_2TNPP	−6.08	−3.34	388.92	0.5220	HOMO-1 → LUMO+5
H_2TAPP	−4.73	−2.10	416.55	0.6231	HOMO-1 → LUMO+1
ZnTXPP					
ZnTPP	−4.99	−2.11	377.91	1.3045	HOMO-1 → LUMO
			377.87	1.3089	HOMO-1 → LUMO+1
ZnT(Me)PP	−5.08	−2.25	380.26	1.3790	HOMO-1 → LUMO+1
			380.15	1.3785	HOMO-1 → LUMO
ZnT(MeO)PP	−4.98	−2.20	389.49	1.2444	HOMO-1 → LUMO+1
			388.98	1.2129	HOMO-1 → LUMO
ZnT(F)PP	−5.22	−2.33	382.16	1.3080	HOMO-1 → LUMO+1
			382.16	1.3077	HOMO-1 → LUMO
ZnT(Cl)PP	−5.54	−2.72	381.75	1.4111	HOMO-1 → LUMO+1
			381.59	1.3948	HOMO-1 → LUMO
ZnT(Br)PP	−5.55	−2.70	380.51	1.4496	HOMO-1 → LUMO+1
			380.49	1.4478	HOMO-1 → LUMO
ZnTCPP	−5.57	−2.73	385.72	1.3631	HOMO-1 → LUMO
			385.69	1.3635	HOMO-1 → LUMO+1
ZnTSPP	−5.96	−3.12	382.76	1.4584	HOMO-1 → LUMO
			382.50	1.4579	HOMO-1 → LUMO+1
ZnTNPP	−5.91	−3.08	376.07	1.1103	HOMO-1 → LUMO
			376.04	1.1029	HOMO-1 → LUMO+1
ZnTAPP	−4.77	−2.02	366.71	0.8636	HOMO-5 → LUMO
			366.53	0.8557	HOMO-5 → LUMO+1

withdrawing nature of carboxyl substituent, ZnTCPP does not have strong interaction with Ag NPs in compare with ZnTAPP. The NH_2 electron donating groups are enable to make stronger interaction. The mentioned observation confirms that porphyrin substituents play a role in the interaction with the surface of Ag NPs. The increased absorption

Table 2
The energy levels of frontier orbitals and the main excitation properties for the ZnTXPP-AgNPs. HOMO/LUMO energy unit: eV. The (U)B3LYP method by using 6-311G(d) basis sets for all atoms except Ag and LANL2DZ basis sets for Ag atom is used to perform both structure optimization and time-dependent density-functional theory (TD-DFT) calculations.

	HOMO	LUMO	Wavelength (nm)	f (oscillating strength)	Orbitals
ZnT(MeO)PP-AgNPs	−4.74	−2.24	551.35	0.0216	HOMO-1 → LUMO
			550.24	0.0179	HOMO → LUMO+1
ZnT(F)PP-AgNPs	−4.94	−2.62	545.86	0.0133	HOMO-1 → LUMO
			545.69	0.0120	HOMO-1 → LUMO+1
ZnT(Cl)PP-AgNPs	−4.96	−2.73	542.73	0.0103	HOMO-1 → LUMO
			541.79	0.0069	HOMO-1 → LUMO+1
ZnT(Br)PP-AgNPs	−4.87	−2.74	547.37	0.0191	HOMO-1 → LUMO
			547.03	0.0172	HOMO-1 → LUMO+1
ZnTCPP-AgNPs	−4.06	−2.89	838.19	0.0464	HOMO → LUMO+2
ZnTSPP-AgNPs	−4.48	−3.14	542.22	0.0098	HOMO-2 → LUMO+1
			541.96	0.0079	HOMO-1 → LUMO+1
ZnTNPP-AgNPs	−4.70	−3.32	1233.68	0.2293	HOMO → LUMO
ZnTAPP-AgNPs	−4.03	−2.13	424.45	0.0694	HOMO → LUMO+3

of dye molecules observed in some of the porphyrin-AgNPs systems could be occurred due to the increased light scattering induced by LSPs, which increased the optical path. Also, these observations could be related to the probable interaction of dye molecular dipole and enhanced electric field surrounding the plasmonic NPs.

In the case of ZnTPP-AgNPs, ZnT(Me)PP-AgNPs, ZnT(F)PP-AgNPs, ZnT(Cl)PP-AgNPs, ZnT(Br)PP-AgNPs, ZnTCPP-AgNPs, and ZnTNPP-AgNPs that create donor-acceptor systems, red-shifted broad absorption is observable due to charge-transfer bands [63,64]. ZnT(MeO)PP-AgNPs, ZnTSPP-AgNPs, and ZnTAPP-AgNPs, are showing blue-shifted broad absorption because of charge-transfer bands. Charge transfer absorption observed in porphyrin-AgNPs systems is evidence of charge-transfer complexation between porphyrin-silver NPs systems. In the ZnTCPP-AgNPs, ZnTSPP-AgNPs, ZnTNPP-AgNPs and ZnTAPP-AgNPs systems, chemisorption of porphyrin molecule to Ag NPs could be occurred due to the presence of anchor groups on porphyrin. The $–CO_2H$, $–SO_3H$, $–NO_2$, and $–NH_2$ functional groups of porphyrin molecules allow ZnTCPP, ZnTSPP, ZnTNPP, and ZnTAPP to be strongly adsorbed on the surface of Ag NPs, respectively. Therefore, the noticeable red-shifted absorption in ZnTCPP-AgNPs and ZnTNPP-AgNPs, and the blue-shifted absorption in ZnTSPP-AgNPs and ZnTAPP-AgNPs has been assigned as charge transfer band arising from the interaction between ZnTXPP and Ag NPs.

Absorption spectra of ZnTPP-Ag@ZIF-8, ZnT(Me)PP-Ag@ZIF-8, ZnT(MeO)PP-Ag@ZIF-8, ZnT(F)PP-Ag@ZIF-8, ZnT(Cl)PP-Ag@ZIF-8, ZnT(Br)PP-Ag@ZIF-8, ZnTCPP-Ag@ZIF-8, ZnTSPP-Ag@ZIF-8, ZnTNPP-Ag@ZIF-8, and ZnTAPP-Ag@ZIF-8, are examined and the resulted data are presented in Fig. S5 (ESI). From the obtained data, it was found that no noticeable shift in the absorption of ZnTXPP is observable in the presence of Ag@ZIF-8 for all of the studied porphyrins. As mentioned previously, the red-shifted absorption in ZnTCPP-AgNPs and the blue-shifted absorption in ZnTAPP-AgNPs related to ZnTCPP and ZnTAPP, respectively, has been assigned as charge transfer band arising from the chemisorption of ZnTCPP and ZnTAPP molecule to Ag NPs. But, in the ZnTCPP-Ag@ZIF-8 and ZnTAPP-Ag@ZIF-8 system, considerable

shifting in the absorption is not observed due to the lack of charge-transfer bands in the presence of ZIF-8 shell around of Ag NPs, which confirmed Ag NPs is surrounded with a uniform and continuous ZIF-8 shell.

To investigate the plasmonic effect on device performance, we compared the performance of plasmon-enhanced PSSCs and standard PSSCs with only ZnTXPP and ZnTXPP-AgNPs as the sensitizing systems. The ZnTXPP-only PSSCs were fabricated using immersion of photoanode in the solution of ZnTXPP, while the ZnTXPP-AgNPs were used as a sensitizer to fabricate the plasmon-enhanced PSSCs. The photocurrent density voltage characteristics (J-V curves) of the plasmon-enhanced PSSCs and ZnTXPP-dyed-only PSSCs with the same photoanode thickness, are presented in Fig. 5 and Fig. 6. As seen in Table 3 and Table 4, the ZnTCPP-dyed-only PSSCs showed a PCE (η) of 1.05%, whereas the plasmon-enhanced PSSCs dyed with ZnTCPP-AgNPs exhibited a PCE of 3.14% (increased by about 200%). Compared with the ZnTCPP-dyed only PSSCs, the fill factor (FF) of the plasmon-enhanced PSSCs was close, while the short-circuit current density (J_{SC}) significantly increased by about 150%, from 3.51 mA cm^{-2} to 8.77 mA cm^{-2}. Also, open-circuit voltage (V_{OC}) was increased by about 20%, from 0.55 V to 0.66 V. Since overall conversion efficiency (η) = $J_{SC}.V_{OC}.FF/P_0$, where P_0 is the intensity of incident light, the improvement of PCE in the plasmon-enhanced PSSCs is mainly due to the increased photocurrent corresponding to enhanced dye absorption by the plasmonic effect. Fig. S4 shows the absorption spectra of Ag NPs and ZnTCPP-AgNPs. The Ag NPs exhibit surface plasmon absorption in the visible area, confirming the plasmonic activity of Ag NPs. As can be seen from Fig. S4, the absorption bands of ZnTCPP and ZnTCPP-AgNPs seen at 424 and 438 nm, respectively; the ZnTCPP-AgNPs is showing red-shift as compared to the ZnTCPP. Also, ZnTCPP-AgNPs is showing significant broadening Soret and Q-band absorbance compared to ZnTCPP.

The cell parameters of the PSSCs employing ZnTXPP- and ZnTXPP-AgNPs-loaded TiO_2 photoanodes are summarized in Tables 3 and 4, and the J-V characteristics of the prepared cells are presented in Figs. 5 and 6. ZnTPP is used as base porphyrin to compare cell characteristics of functionalized porphyrin with various electron-donating and electron-withdrawing substituents. Excluding the magnitude, the trends observed in the photocurrents and photovoltages for porphyrins containing electron withdrawing substituents with inductive effect were similar to unsubstituted porphyrin ZnTPP. The PSSCs employing ZnT(MeO)PP-loaded TiO_2 as photoanode, in which methoxy is electron withdrawing substituent with inductive effect, show an slight increase in short-circuit current compared to ZnTPP. In contrast, the open-circuit voltage of the PSSCs containing ZnT(MeO)PP dye is similar to the ones employing ZnTPP-loaded TiO_2 as a photoanode. Distinctively, different trends were seen in DSSCs that employed porphyrins consisting electron withdrawing and electron donating substituents with resonance effect as a dye. The DSSC employing the photoanode sensitized by ZnTCPP dye exhibits noticeable changes in the photocurrent from 1.05 $mAcm^{-2}$ (ZnTPP-loaded TiO_2 as photoanode) to 3.51 $mAcm^{-2}$ (ZnTCPP-loaded TiO_2 as photoanode) with an increase of 98 mV in open-circuit voltage as compared to the ZnTPP-sensitized photoanode. Changes in the cell characteristics with photoanode sensitized by ZnTAPP dye relative to ZnTPP are also considerable from 1.05 mA cm^{-2} (ZnTPP-loaded TiO_2) to 3.07 mA cm^{-2} (ZnTAPP-loaded TiO_2) in photocurrents and 78 mV increasing in photovoltage. The significant increase in V_{OC} observed in PSSCs employing ZnTCPP- and ZnTAPP-loaded TiO_2 as photoanode confirmed that a mechanism other than electron-induced effect is also operative in determining the performance of DSSCs. The mentioned mechanism includes the nature of carboxyl and amine functional groups to chemisorb by TiO_2. Chemisorption of ZnTCPP and/or ZnTAPP onto TiO_2 lead to increasing the concentration of loaded dye and consequently an increase in absorption of the incident light. Chemisorption versus electronic effect in PSSCs is observable in other prepared cells, as presented in Table 3 and Fig. 5.

As it is observable in Fig. 6 and Table 4, the cell characteristics have distinctively different trends in the case of ZnTXPP-AgNPs-sensitized cells relative to ZnTXPP-sensitized ones, which plasmonic versus electronic effect is responsible to the observed results. The results is showing an increase in V_{OC} for ZnTPP-AgNPs relative to ZnTPP, but a noticeable decrease in the J_{SC}, FF, and η of ZnTPP-AgNPs. The similar trends are observable for ZnT(MeO)PP and ZnT(MeO)PP-AgNPs sensitized solar cells.

The photovoltaic parameters of ZnT(F)PP and ZnT(F)PP-AgNPs are showing an improvement in cell characteristics of ZnT(F)PP-AgNPs relative to ZnT(F)PP-sensitized one. Plasmon-induced enhancement of light absorption and enhancement in photoconversion efficiency induced by plasmonic effect are responsible for observed results. Also, plasmon-induced increasing light absorption and photoconversion efficiency is observable for ZnT(Me)PP-AgNPs, ZnT(Cl)PP-AgNPs, and ZnT

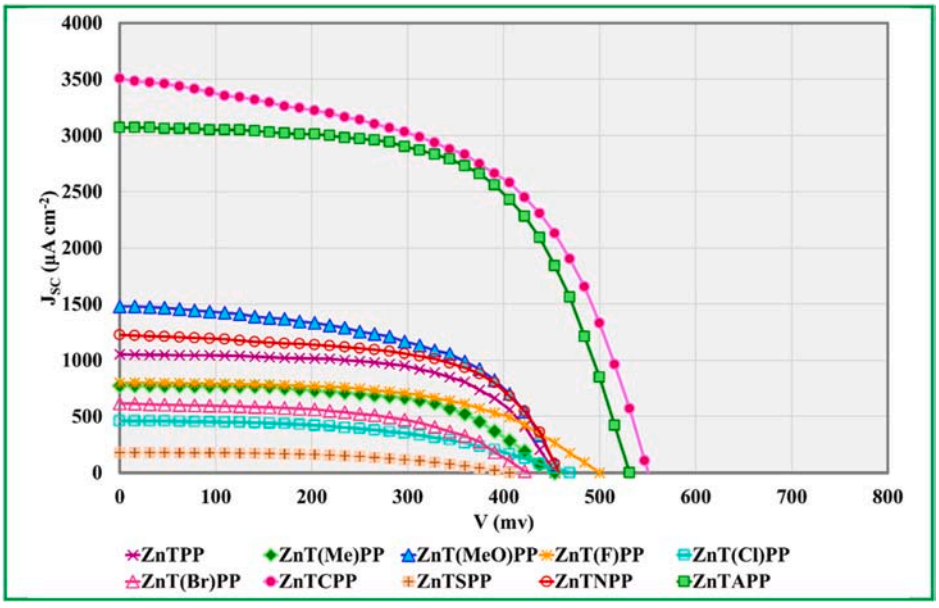

Fig. 5. J-V curves of the PSSCs using the ZnTXPP-loaded TiO_2 as the photoanodes under irradiation intensity of 1 sun (100 $mWcm^{-2}$, AM1.5). (The figures including error bars are provided in ESI.)

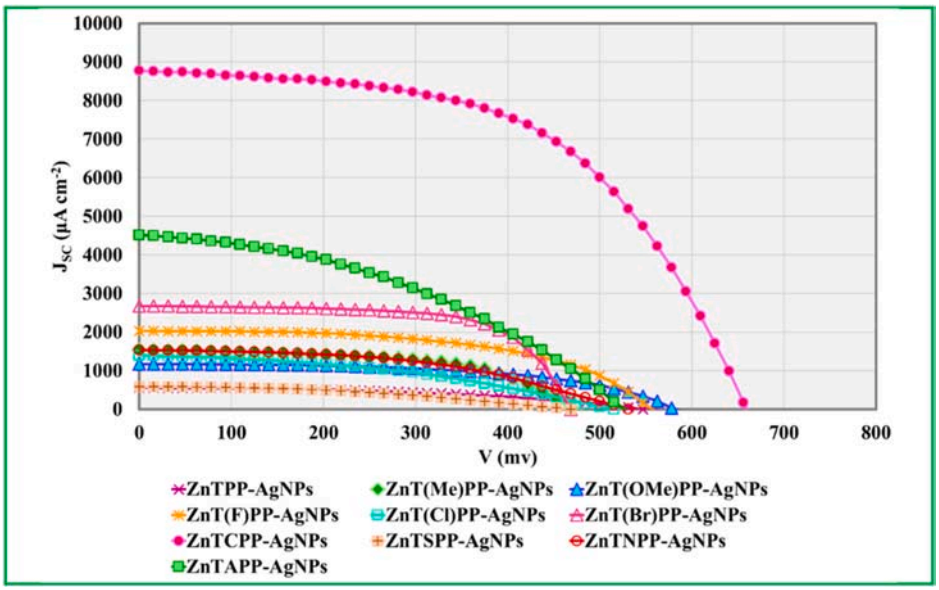

Fig. 6. J-V curves of the PSSCs using the ZnTXPP-AgNPs-loaded TiO_2 under irradiation intensity of 1 sun (100 mWcm^{-2}, AM1.5). (The figures including error bars are provided in ESI.)

Table 3
Characteristic values of the PSSCs using the ZnTXPP-loaded TiO_2 as the photoanodes under irradiation intensity of 1 sun (100 mWcm^{-2}, AM1.5).

Electrode	J_{SC} (mAcm^{-2})	V_{OC} (mV)	FF	η (%)
ZnTPP	1.05	453	0.61	0.29
ZnT(Me)PP	0.77	453	0.58	0.20
ZnT(MeO)PP	1.48	457	0.54	0.36
ZnT(F)PP	0.80	500	0.55	0.22
ZnT(Cl)PP	0.46	469	0.48	0.10
ZnT(Br)PP	0.62	427	0.53	0.14
ZnTCPP	3.51	551	0.54	1.05
ZnTSPP	0.18	406	0.49	0.04
ZnTNPP	1.23	458	0.60	0.33
ZnTAPP	3.07	531	0.61	1.00

Table 4
Characteristic values of the PSSCs using the ZnTXPP-AgNPs-loaded TiO_2 as the photoanodes under irradiation intensity of 1 sun (100 mWcm^{-2}, AM1.5).

Electrode	J_{SC} (mAcm^{-2})	V_{OC} (mV)	FF	η (%)
ZnTPP-AgNPs	0.55	547	0.44	0.13
ZnT(Me)PP-AgNPs	1.54	471	0.55	0.40
ZnT(MeO)PP-AgNPs	1.17	583	0.54	0.37
ZnT(F)PP-AgNPs	2.03	557	0.54	0.61
ZnT(Cl)PP-AgNPs	1.39	516	0.40	0.28
ZnT(Br)PP-AgNPs	2.67	469	0.66	0.83
ZnTCPP-AgNPs	8.77	660	0.54	3.14
ZnTSPP-AgNPs	0.58	469	0.40	0.11
ZnTNPP-AgNPs	1.53	531	0.46	0.38
ZnTAPP-AgNPs	4.51	528	0.39	0.93

(Br)PP-AgNPs, as it is presented in Table 4. In the normal DSSCs, charge injection from the excited dye into TiO_2 nanoparticles is done in photoanode, and solar cell performance is continued by the transport of electrons to the collecting electrode surface. When ZnTXPP-AgNPs are presented as the loaded dye in photoanode, localized plasmonic effects on the absorption of dye effect on cell characteristics.

From the obtained data, V_{OC} in PSSCs in the presence of ZnTXPP-AgNPs is increased relative to porphyrin ones except ZnTAPP-AgNPs. The PSSCs employing ZnTXPP-AgNPs exhibit an increment in open-circuit voltage as compared to the ZnTXPP photoanode with noticeable changes in the photocurrent (Fig. 6). In the case of ZnTCPP-AgNPs, the significant increase in V_{OC} is observable relative to another ZnTXPP-AgNPs systems; it is suggesting that the performance of DSSCs is influenced by other mechanisms than plasmon-induced enhancement. In the systems with Ag NPs in contact with dye molecules, TiO_2 nanoparticles are accepting electrons from the ZnTXPP-AgNPs. PNPs store a fraction of electrons captured from photo-excited semiconductor NPs and does not quickly discharge electrons to the surrounding medium; as a result, they achieve to a charge equilibration with a photo-excited semiconductor and drives the Fermi level to more negative potentials [65,66]. Fermi level equilibration in the mentioned systems lead to shift of the apparent Fermi level to a more negative potential, and consequently, an increase in the open-circuit voltage of the DSSCs [65]. It is reported that Ag NPs contacted with TiO_2 NPs capture electrons from photoexcited TiO_2 NPs and resulting in the storage of electrons by Ag NPs. Electron stored by Ag NPs undergoes charge equilibration with a photoexcited TiO_2 NPs and drives the Fermi level to more negative potentials [65]. Also, stored electrons by Ag NPs have another influence on the performance of DSSCs using prevention of back electron transfer [65]. Therefore, the significant increases in V_{OC} of ZnTCPP-AgNPs is probably due to electron storage in Ag NPs and chemically absorption of ZnTCPP molecules on the surface of Ag NPs. From the results (Fig. 6 and Table 4), the PSSCs employing ZnTXPP-AgNPs as photoanode show changing in short-circuit current relative to ZnTXPP. The change in photocurrent is relevant to the nature of the substituent of porphyrins.

The light absorption of the porphyrin molecules in the Soret and Q-bands are strong, but in the other spectral region, the absorption of the porphyrin is not noticeable. As mentioned previously, using ZnTCPP-AgNPs and ZnTAPP-AgNPs systems, improved light harvesting is occurring by broadening and shifting of the absorbance of the Soret and Q-bands. ZnTCPP-AgNPs is showing significant broadening and shifting of Soret and Q-band absorbance compared to ZnTPP-AgNPs, yielding improved light harvesting in the blue and green regions of the spectrum. ZnTAPP-AgNPs is also demonstrating broadening and shifting in light absorption. The enhancement in light absorption of ZnTCPP-AgNPs is resulted in improved J_{SC} (3.51 versus 8.77 mA cm^{-2} for ZnTCPP and ZnTCPP-AgNPs, respectively) when utilized in the PSSCs [13,35].

As it is reported, the DSSCs are promising candidates for the conversion of weak light to electricity [67–69], the cell efficiencies using the ZnTCPP-AgNPs-loaded TiO_2 as the photoanode were measured under irradiation intensity of 1, 1/2, and 1/4 sun (AM1.5), and detailed cell parameters are collected in Table 5 and Fig. 7. From the obtained results,

Table 5
Detailed photovoltaic parameters of PSSCs using the ZnTCPP-AgNPs-loaded TiO_2 as the photoanode measured at a set of incident light intensities.

Incident power intensity (P_{in})	J_{SC} ($mAcm^{-2}$)	V_{OC} (mV)	FF	η (%)
1/4 SUN	2.64	609	0.50	3.22
1/2 SUN	4.58	645	0.54	3.17
1 SUN	8.77	660	0.54	3.14

the cell performance is considerable at a light intensity of 1/4 SUN.

To further investigate the plasmonic effect on device performance, the performance of plasmon-enhanced PSSCs using ZnTXPP-AgNPs and/or ZnTXPP-Ag@ZIF-8 as sensitizer was compared. The ZnTXPP-Ag@ZIF-8 were prepared using a coating of the Ag core by the shell of ZIF-8. The photocurrent density voltage characteristics (J-V curves) of the plasmon-enhanced DSSCs using ZnTXPP-Ag@ZIF-8 are presented in Fig. 8 and Table 6. The ZnTPP-Ag@ZIF-8 showed a PCE(η) of 0.11%, whereas the ZnTPP-AgNPs exhibited a PCE of 0.13% (decreased by 15%). Compared with the ZnT(Br)PP-dyed-only DSSC, the FF and V_{OC} of the ZnT(Br)PP-Ag@ZIF-8 have small differences in magnitude (FF increased by 7% and V_{OC} increased by 10%), while the J_{SC} increased by 56%, from 0.62 $mAcm^{-2}$ to 0.97 $mAcm^{-2}$. Since $\eta = J_{SC}.V_{OC}.FF/P_0$, the improvement of PCE in the ZnT(Br)PP-Ag@ZIF-8 system is mainly due to the increased J_{SC} corresponding to enhanced dye absorption by the plasmonic effect.

The open-circuit voltage of DSSCs employing ZnTXPP-Ag@ZIF-8 as photoanode is more than the one employing ZnTXPP except ZnTAPP-Ag@ZIF-8. It is reported that ZIF-8 usage in DSSCs to coating TiO_2 NPs results in a significantly increased V_{OC} than none-covered ones, as well as the much higher dye loading in the presence of ZIF-8 on the

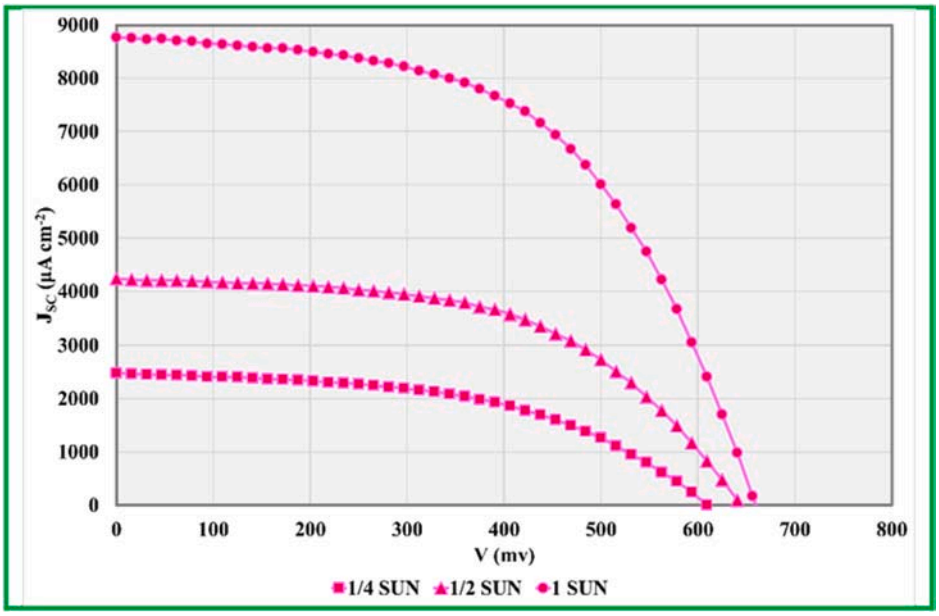

Fig. 7. J-V curves of the PSSCs using the ZnTCPP-AgNPs-loaded TiO_2 under various light intensities of AM1.5 sunlight.

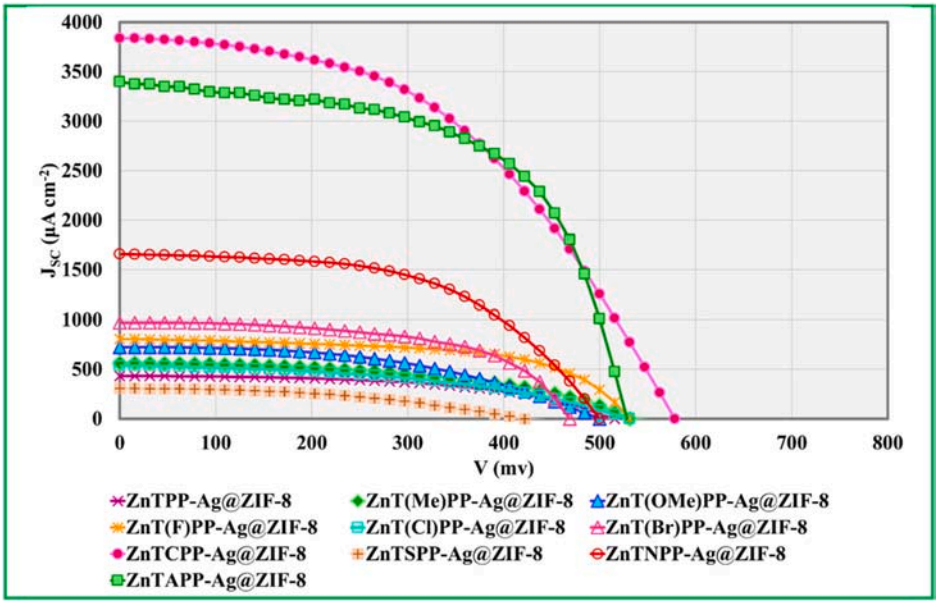

Fig. 8. J-V curves of the PSSCs using the ZnTXPP-Ag@ZIF-8-loaded TiO_2 under irradiation intensity of 1 sun (100 $mWcm^{-2}$, AM1.5). (The figures including error bars are provided in ESI.)

Table 6
Characteristic values of the PSSCs using the ZnTXPP-Ag@ZIF-8-loaded TiO_2 as the photoanodes under irradiation intensity of 1 sun (100 $mWcm^{-2}$, AM1.5).

Electrode	J_{SC} ($mAcm^{-2}$)	V_{OC} (mV)	FF	η (%)
ZnTPP-Ag@ZIF-8	0.43	516	0.52	0.11
ZnT(Me)PP-Ag@ZIF-8	0.56	531	0.48	0.14
ZnT(MeO)PP-Ag@ZIF-8	0.72	500	0.46	0.17
ZnT(F)PP-Ag@ZIF-8	0.80	531	0.59	0.25
ZnT(Cl)PP-Ag@ZIF-8	0.53	531	0.44	0.12
ZnT(Br)PP-Ag@ZIF-8	0.97	469	0.57	0.26
ZnTCPP-Ag@ZIF-8	3.84	578	0.47	1.04
ZnTSPP-Ag@ZIF-8	0.30	422	0.43	0.05
ZnTNPP-Ag@ZIF-8	1.65	500	0.54	0.45
ZnTAPP-Ag@ZIF-8	3.40	528	0.58	1.04

photoanode. Therefore, the DSSCs efficiency was enhanced with the help of the ZIF-8 layer [70–72]. Also, it is reported that MOFs containing photosensitizing organic linkers could be applied as the sensitizer for the photoanodes in DSSCs, but, the photocurrent is still needed to be increased. Sensitization of DSSCs by some MOFs still shows limited cell efficiencies due to the electrically insulating property of these frameworks [73,74]. The utilizing MOFs light-harvesting materials as the sensitizer in photovoltaic devices is still a challenge and it needs further investigation. Therefore, employing MOFs to improve the functioning of the DSSCs must be adapted to achieve performance enhancements. The respectable strategy to improve the performance of MOFs sensitized solar cell may be utilizing modified MOFs-containing systems to achieve a higher conductivity or a faster charge-transport rate in MOFs [70].

To study electron recombination process, electrochemical impedance spectroscopy (EIS) was used. In this study, the R_s is showing the overall series resistance of the corresponding circuit. The obtained EIS Nyquist plots are represented in Fig. S9. Two semicircles can be seen in the plots. The semicircle that is positioned at the right side is related to the charge transfer resistance, R_{ct}, between the dyed-TiO_2/electrolyte interfaces. The results related to the R_{ct} of investigated cells are presented in Table 7. The calculated R_{ct} is 27.94, 35.13, and 32.55 Ω for ZnTCPP, ZnTCPP-AgNPs, and ZnTCPP-Ag@ZIF-8, respectively. The decrease in the R_{ct} is showing an increase in the charge recombination and as a result a lower amount of the V_{OC}. The semicircle at the left hand is showing the charge transfer resistance at the interface of the Pt electrode and electrolyte interface (R_{Pt}). Based on the results presented in Fig. S9 the change in the R_{Pt} is not in a considerable amount, because of the similarity of the Pt electrode and electrolyte in the devices.

The electron lifetime can be calculated by using the equation $\tau_n = R_{ct} \times C_\mu$, in which the C_μ is chemical capacitance. The calculated lifetime for cells sensitized by ZnTCPP, ZnTCPP-AgNPs, and ZnTCPP-Ag@ZIF-8 are 29.29, 34.75, and 37.56 ms, respectively.

In the prepared PSSCs, I^-/I_3^- was employed as the redox shuttle. In PSSCs, I^-/I_3^- allowed to come into direct contact with the ZnTXPP-AgNPs and ZnTXPP-Ag@ZIF-8 nanostructures which can etched them since I^-/I_3^- is extremely corrosive toward Ag NPs. The etching of Ag NPs will changed the characteristic absorption feature of the prepared systems [36]. To examine the stability of the fabricated cells, the prepared ZnTCPP-AgNPs and ZnTCPP-Ag@ZIF-8 hybrid nanostructures were exposed to the electrolyte. The changes in the intense absorption of ZnTCPP in the prepared ZnTCPP-AgNPs and ZnTCPP-Ag@ZIF-8 nanostructures after a 16 h of exposure to I^-/I_3^- can be used to determine the stability of the fabricated cells.

Table 7
Parameters obtained by fitting the impedance spectra of the PSSCs with sensitizers.

Sensitizers	R_s (Ω)	R_{ct} (Ω)	R_{Pt} (Ω)	τ_n (ms)
ZnTCPP	5.50	27.94	4.09	29.29
ZnTCPP-AgNPs	5.51	35.13	4.08	34.75
ZnTCPP-Ag@ZIF-8	5.52	32.55	4.06	37.56

As mentioned earlier, red-shifted broad absorption is observable in ZnTCPP-AgNPs relative to ZnTCPP, due to charge-transfer between molecular-silver NPs system. When I^-/I_3^- in the electrolyte allowed to come into direct contact with the ZnTCPP-AgNPs, the characteristic absorption feature of the system was changed (Fig. S10). But, no noticeable shift in the absorption of ZnTCPP-Ag@ZIF-8 is observable after a 24 h of exposure to I^-/I_3^- in the electrolyte. The change in the red-shifted broad absorption of ZnTCPP in the prepared ZnTCPP-AgNPs after a short period of time of exposure to I^-/I_3^- showed that the stability of the fabricated cell using ZnTCPP-AgNPs is lower than ZnTCPP-Ag@ZIF-8 one (Fig. S10). In the case of Ag@ZIF-8, a shell layer of ZIF-8 isolates the Ag NPs from I^-/I_3^-, preserving silver nanoparticles.

To perform the stability test of the cells, two different test were performed. In one series, the cell including ZnTCPP-AgNPs were used. The data related to the prepared cell immediately after cell assembly and after 7 days is provided in Table 8 and Figure S11 (ESI). The results are showing that the performance of cell is decreased in a considerable amount. In this case, the reaction between the Ag NPs and electrolyte cause to destroy the Ag NPs; in this situation, there is less improvement of cell efficiency *via* plasmonic effect. In other case, the cell including ZnTCPP-Ag@ZIF-8 is analyzed immediately after cell assembly and after 7 days. In this case, the ZIF-8 is playing its role to protect the Ag NPs from contact with electrolyte; as a result, the Ag NPs can perform their role to improve the cell performance after the mentioned time.

4. Conclusion

The LSPR of Ag NPs was used to improve the light absorption of porphyrins in plasmon-enhanced PSSCs. Porphyrins with different substituents consisting –H (as base porphyrin), -Me, -MeO, –F, -Cl, -Br, $–CO_2H$, $–SO_3H$, $–NO_2$, and $–NH_2$ were selected and used to study the effect of light-harvesting donor and/or acceptor dyes in conjunction with plasmonic nanoparticles on the performance of PSSCs. The obtained results revealed that the performance of PSSCs by using porphyrins with electron withdrawing substituents are better than PSSCs containing electron donating groups. ZnTCPP and ZnTAPP dyes have made the biggest impact on the performance of plasmon-enhanced PSSCs due to their ability to chemically absorb on the surface of Ag NPs. Computational studies were applied to examine the electronic properties of porphyrin molecules with various substituents interacted with Ag NPs, which indicated that the electronic nature of substituents has a noticeable effect on the electronic properties of porphyrin-AgNPs systems. Furthermore, Ag@ZIF-8 core-shell NPs were used to prevent corrosion of Ag PNPs. Also, Ag@ZIF-8 was used as the scattering component of photoanode in PSSCs to improve light absorption. From the obtained data, porphyrin-Ag@ZIF-8 systems improved the performance of PSSCs relative to corresponding porphyrins but the results were not as good as porphyrin-AgNPs systems.

CRediT authorship contribution statement

Rahim Ghadari: Conceptualization, Funding acquisition, Investigation, Project administration, Writing – original draft. **Alireza Sabri:**

Table 8
Characteristic values of the PSSCs using the ZnTCPP-AgNPs and ZnTCPP-Ag@ZIF-8 sensitizing systems after cell assembly and after 7 days under irradiation intensity of 1 sun (100 $mWcm^{-2}$, AM1.5).

Electrode		J_{SC} ($mAcm^{-2}$)	V_{OC} (mV)	FF	η (%)
ZnTCPP-AgNPs	after cell assembly	9.01	657	0.51	3.02
	after 7 days	6.83	637	0.50	2.17
ZnTCPP-Ag@ZIF-8	after cell assembly	3.91	583	0.47	1.07
	after 7 days	3.77	579	0.47	1.02

Investigation, Methodology, Data curation. **Paria-Sadat Saei:** Investigation, Methodology, Data curation. **Fantai Kong:** Writing – review & editing. **Yousef Mohammadzadeh:** Methodology. **Emre Guzel:** Formal analysis.

Declaration of competing interest

The authors declare that they have no known competing financial interests or personal relationships that could have appeared to influence the work reported in this paper.

Acknowledgment

This work is supported by the CAS-Iranian Vice Presidency for Science and Technology Joint Research Project (no. 96003452). The support from the research council of University of Tabriz is acknowledged, as well.

Appendix A. Supplementary data

Supplementary data to this article can be found online at https://doi.org/10.1016/j.jpowsour.2021.230407.

References

[1] K. Kakiage, Y. Aoyama, T. Yano, K. Oya, J. Fujisawa, M. Hanaya, Highly-efficient dye-sensitized solar cells with collaborative sensitization by silyl-anchor and carboxy-anchor dyes, Chem. Commun. 51 (2015) 15894–15897, https://doi.org/10.1039/C5CC06759F.

[2] M. Grätzel, Conversion of sunlight to electric power by nanocrystalline dye-sensitized solar cells, J. Photochem. Photobiol. Chem. 164 (2004) 3–14, https://doi.org/10.1016/J.JPHOTOCHEM.2004.02.023.

[3] J. Qi, X. Dang, P.T. Hammond, A.M. Belcher, Highly efficient plasmon-enhanced dye-sensitized solar cells through Metal@Oxide core–shell nanostructure, ACS Nano 5 (2011) 7108–7116, https://doi.org/10.1021/nn201808g.

[4] S. Mathew, A. Yella, P. Gao, R. Humphry-Baker, B.F.E. Curchod, N. Ashari-Astani, I. Tavernelli, U. Rothlisberger, M.K. Nazeeruddin, M. Grätzel, Dye-sensitized solar cells with 13% efficiency achieved through the molecular engineering of porphyrin sensitizers, Nat. Chem. 6 (2014) 242–247, https://doi.org/10.1038/nchem.1861.

[5] H.J. Snaith, L. Schmidt-Mende, Advances in liquid-electrolyte and solid-state dye-sensitized solar cells, Adv. Mater. 19 (2007) 3187–3200, https://doi.org/10.1002/adma.200602903.

[6] Juan Bisquert, David Cahen, Gary Hodes, Sven Rühle, Arie Zaban, Physical chemical principles of photovoltaic conversion with nanoparticulate, mesoporous dye-sensitized solar cells, J. Phys. Chem. B 108 (2004) 8106–8118, https://doi.org/10.1021/JP0359283.

[7] T. Hamamura, J.T. Dy, K. Tamaki, J. Nakazaki, S. Uchida, T. Kubo, H. Segawa, Dye-sensitized solar cells using ethynyl-linked porphyrin trimers, Phys. Chem. Chem. Phys. 16 (2014) 4551–4560, https://doi.org/10.1039/c3cp55184a.

[8] B. O'Regan, M. Grätzel, A low-cost, high-efficiency solar cell based on dye-sensitized colloidal TiO2 films, Nature 353 (1991) 737–740, https://doi.org/10.1038/353737a0.

[9] M. Grätzel, Photoelectrochemical cells, Nature 414 (2001) 338–344, https://doi.org/10.1038/35104607.

[10] M.K. Nazeeruddin, A. Kay, I. Rodicio, R. Humphry-Baker, E. Mueller, P. Liska, N. Vlachopoulos, M. Graetzel, Conversion of light to electricity by cis-X2bis(2,2'-bipyridyl-4,4'-dicarboxylate)ruthenium(II) charge-transfer sensitizers (X = Cl-, Br-, I-, CN-, and SCN-) on nanocrystalline titanium dioxide electrodes, J. Am. Chem. Soc. 115 (1993) 6382–6390, https://doi.org/10.1021/ja00067a063.

[11] C.-Y. Chen, M. Wang, J.-Y. Li, N. Pootrakulchote, L. Alibabaei, C. Ngoc-le, J.-D. Decoppet, J.-H. Tsai, C. Grätzel, C.-G. Wu, S.M. Zakeeruddin, M. Grätzel, Highly efficient light-harvesting ruthenium sensitizer for thin-film dye-sensitized solar cells, ACS Nano 3 (2009) 3103–3109, https://doi.org/10.1021/nn900756s.

[12] M. Grätzel, Dye-sensitized solar cells, J. Photochem. Photobiol. C Photochem. Rev. 4 (2003) 145–153, https://doi.org/10.1016/S1389-5567(03)00026-1.

[13] B.E. Hardin, E.T. Hoke, P.B. Armstrong, J.-H. Yum, P. Comte, T. Torres, J.M. J. Fréchet, M.K. Nazeeruddin, M. Grätzel, M.D. McGehee, Increased light harvesting in dye-sensitized solar cells with energy relay dyes, Nat. Photonics 3 (2009) 406–411, https://doi.org/10.1038/nphoton.2009.96.

[14] S. Chang, Q. Li, X. Xiao, K.Y. Wong, T. Chen, Enhancement of low energy sunlight harvesting in dye-sensitized solar cells using plasmonic gold nanorods, Energy Environ. Sci. 5 (2012) 9444–9448, https://doi.org/10.1039/c2ee22657j.

[15] B.E. Hardin, E.T. Hoke, P.B. Armstrong, J.-H. Yum, P. Comte, T. Torres, J.M. J. Fréchet, M.K. Nazeeruddin, M. Grätzel, M.D. McGehee, Increased light harvesting in dye-sensitized solar cells with energy relay dyes, Nat. Photonics 3 (2009) 406–411, https://doi.org/10.1038/nphoton.2009.96.

[16] Mohammad K. Nazeeruddin, Filippo De Angelis, Simona Fantacci, Annabella Selloni, Viscardi Guido, Seigo Ito, Bessho Takeru, M. Grätzel, Combined experimental and DFT-TDDFT computational study of photoelectrochemical cell ruthenium sensitizers, J. Am. Chem. Soc. 127 (2005) 16835–16847, https://doi.org/10.1021/JA052467L.

[17] J.-J. Cid, J.-H. Yum, S.-R. Jang, M.K. Nazeeruddin, E. Martínez-Ferrero, E. Palomares, J. Ko, M. Grätzel, T. Torres, Molecular cosensitization for efficient panchromatic dye-sensitized solar cells, Angew. Chem. 119 (2007) 8510–8514, https://doi.org/10.1002/ange.200703106.

[18] S.A. Haque, Y. Tachibana, R.L. Willis, J.E. Moser, M. Grätzel, D.R. Klug, J. R. Durrant, Parameters influencing charge recombination kinetics in dye-sensitized nanocrystalline titanium dioxide films, J. Phys. Chem. B 104 (2000) 538–547, https://doi.org/10.1021/jp991085x.

[19] B.C. O'Regan, K. Walley, M. Juozapavicius, A. Anderson, F. Matar, T. Ghaddar, S. M. Zakeeruddin, C. Klein, J.R. Durrant, Structure/function relationships in dyes for solar energy conversion: a two-atom change in dye structure and the mechanism for its effect on cell voltage, J. Am. Chem. Soc. 131 (2009) 3541–3548, https://doi.org/10.1021/ja806869x.

[20] Brian C. O'Regan, Ismael López-Duarte, M. Victoria Martínez-Díaz, Amparo Forneli, Josep Albero, Ana Morandeira, Emilio Palomares, Tomás Torres, J.R. Durrant, Catalysis of recombination and its limitation on open circuit voltage for dye sensitized photovoltaic cells using phthalocyanine dyes, J. Am. Chem. Soc. 130 (2008) 2906–2907, https://doi.org/10.1021/JA078045O.

[21] H. Wang, M. Liu, M. Zhang, P. Wang, H. Miura, Y. Cheng, J. Bell, Kinetics of electron recombination of dye-sensitized solar cells based on TiO2 nanorod arrays sensitized with different dyes, Phys. Chem. Chem. Phys. 13 (2011) 17359–17366, https://doi.org/10.1039/c1cp22482d.

[22] K. Sharma, V. Sharma, S.S. Sharma, Dye-sensitized solar cells: fundamentals and current status, Nanoscale Res. Lett. 13 (2018) 381, https://doi.org/10.1186/s11671-018-2760-6.

[23] H.A. Atwater, A. Polman, Plasmonics for improved photovoltaic devices, Nat. Mater. 9 (2010) 205–213, https://doi.org/10.1038/nmat2629.

[24] J.-L. Wu, F.-C. Chen, Y.-S. Hsiao, F.-C. Chien, P. Chen, C.-H. Kuo, M.H. Huang, C.-S. Hsu, Surface plasmonic effects of metallic nanoparticles on the performance of polymer bulk heterojunction solar cells, ACS Nano 5 (2011) 959–967, https://doi.org/10.1021/nn102295p.

[25] M.M. Rahman, S.H. Im, J.-J. Lee, Enhanced photoresponse in dye-sensitized solar cells via localized surface plasmon resonance through highly stable nickel nanoparticles, Nanoscale 8 (2016) 5884–5891, https://doi.org/10.1039/C5NR08155F.

[26] S.P. Lim, A. Pandikumar, N.M. Huang, H.N. Lim, G. Gu, T.L. Ma, Promotional effect of silver nanoparticles on the performance of N-doped TiO2 photoanode-based dye-sensitized solar cells, RSC Adv. 4 (2014) 48236–48244, https://doi.org/10.1039/c4ra09775k.

[27] S.P. Lim, A. Pandikumar, N.M. Huang, H.N. Lim, Enhanced photovoltaic performance of silver@titania plasmonic photoanode in dye-sensitized solar cells, RSC Adv. 4 (2014) 38111–38118, https://doi.org/10.1039/c4ra05689b.

[28] K.B. Bhojanaa, M. Ramesh, A. Pandikumar, Complementary properties of silver nanoparticles on the photovoltaic performance of titania nanospheres based photoanode in dye-sensitized solar cells, Mater. Res. Bull. 122 (2020) 110672, https://doi.org/10.1016/j.materresbull.2019.110672.

[29] A. Pandikumar, S.P. Lim, S. Jayabal, N.M. Huang, H.N. Lim, R. Ramaraj, Titania@gold plasmonic nanoarchitectures: an ideal photoanode for dye-sensitized solar cells, Renew. Sustain. Energy Rev. 60 (2016) 408–420, https://doi.org/10.1016/j.rser.2016.01.107.

[30] L. Pang, L.M. Freeman, H.M. Chen, Q. Gu, Y. Fainman, Plasmonics in imaging, biodetection, and nanolasers. Handb. Surf. Sci., North-Holland, 2014, pp. 399–428, https://doi.org/10.1016/B978-0-444-59526-3.00014-8.

[31] S.D. Standridge, G.C. Schatz, J.T. Hupp, Distance dependence of plasmon-enhanced photocurrent in dye-sensitized solar cells, J. Am. Chem. Soc. 131 (2009) 8407–8409, https://doi.org/10.1021/ja9022072.

[32] P.V. Kamat, Photophysical, photochemical and photocatalytic aspects of metal nanoparticles, J. Phys. Chem. B 106 (2002) 7729–7744, https://doi.org/10.1021/JP0209289.

[33] W.-Y. Rho, D.H. Song, H.-Y. Yang, H.-S. Kim, B.S. Son, J.S. Suh, B.-H. Jun, Recent advances in plasmonic dye-sensitized solar cells, J. Solid State Chem. 258 (2018) 271–282, https://doi.org/10.1016/J.JSSC.2017.10.018.

[34] A. Henglein, Small-particle research: physicochemical properties of extremely small colloidal metal and semiconductor particles, Chem. Rev. 89 (1989) 1861–1873, https://doi.org/10.1021/cr00098a010.

[35] J. Villanueva-Cab, J.L. Montaño-Priede, U. Pal, Effects of plasmonic nanoparticle incorporation on electrodynamics and photovoltaic performance of dye sensitized solar cells, J. Phys. Chem. C 120 (2016) 10129–10136, https://doi.org/10.1021/acs.jpcc.6b01053.

[36] S.D. Standridge, G.C. Schatz, J.T. Hupp, Toward plasmonic solar cells: protection of silver nanoparticles via atomic layer deposition of TiO $_2$, Langmuir 25 (2009) 2596–2600, https://doi.org/10.1021/la900113e.

[37] M.D. Brown, T. Suteewong, R.S.S. Kumar, V. D'Innocenzo, A. Petrozza, M.M. Lee, U. Wiesner, H.J. Snaith, Plasmonic dye-sensitized solar cells using Core−Shell Metal−Insulator nanoparticles, Nano Lett. 11 (2011) 438–445, https://doi.org/10.1021/nl1031106.

[38] A.D. Adler, F.R. Longo, J.D. Finarelli, J. Goldmacher, J. Assour, L. Korsakoff, A simplified synthesis for meso-tetraphenylporphine, J. Org. Chem. 32 (1967), https://doi.org/10.1021/jo01288a053, 476–476.

[39] A.D. Adler, F.R. Longo, F. Kampas, J. Kim, On the preparation of metalloporphyrins, J. Inorg. Nucl. Chem. 32 (1970) 2443–2445, https://doi.org/10.1016/0022-1902(70)80535-8.

[40] J. Rochford, D. Chu, A. Hagfeldt, E. Galoppini, Tetrachelate porphyrin chromophores for metal oxide semiconductor sensitization: effect of the spacer length and anchoring group position, J. Am. Chem. Soc. 129 (2007) 4655–4665, https://doi.org/10.1021/JA068218U.
[41] E.B. Fleischer, J.M. Palmer, T.S. Srivastava, A. Chatterjee, Thermodyamic and kinetic properties of an iron-porphyrin system, J. Am. Chem. Soc. 93 (1971) 3162–3167, https://doi.org/10.1021/ja00742a012.
[42] Z. Dong, P.J. Scammells, New methodology for the N-demethylation of opiate alkaloids, J. Org. Chem. 72 (2007) 9881–9885, https://doi.org/10.1021/jo071171q.
[43] A. Bettelheim, B.A. White, S.A. Raybuck, R.W. Murray, Electrochemical polymerization of amino-, pyrrole-, and hydroxy-substituted tetraphenylporphyrins, Inorg. Chem. 26 (1987) 1009–1017, https://doi.org/10.1021/ic00254a011.
[44] P. Rothemund, A.R. Menotti, Porphyrin studies. V. [1] the metal complex salts of α,β,γ,δ-tetraphenylporphine, J. Am. Chem. Soc. 70 (1948) 1808–1812, https://doi.org/10.1021/ja01185a047.
[45] G.D. Dorough, J.R. Miller, F.M. Huennekens, Spectra of the metallo-derivatives of α,β,γ,δ-tetraphenylporphine, J. Am. Chem. Soc. 73 (1951) 4315–4320, https://doi.org/10.1021/ja01153a085.
[46] F.R. Longo, M.G. Finarelli, J.B. Kim, The synthesis and some physical properties of *ms* -tetra(pentafluorophenyl)-porphin and *ms* -tetra(pentachlorophenyl)porphin, J. Heterocycl. Chem. 6 (1969) 927–931, https://doi.org/10.1002/jhet.5570060625.
[47] M. Adineh, P. Tahay, M. Ameri, N. Safari, E. Mohajerani, Fabrication and analysis of dye-sensitized solar cells (DSSCs) using porphyrin dyes with catechol anchoring groups, RSC Adv. 6 (2016) 14512–14521, https://doi.org/10.1039/C5RA23584G.
[48] S. Murphy, L. Huang, P.V. Kamat, Charge-transfer complexation and excited-state interactions in porphyrin-silver nanoparticle hybrid structures, J. Phys. Chem. C 115 (2011) 22761–22769, https://doi.org/10.1021/jp205711x.
[49] G. Lu, S. Li, Z. Guo, O.K. Farha, B.G. Hauser, X. Qi, Y. Wang, X. Wang, S. Han, X. Liu, J.S. DuChene, H. Zhang, Q. Zhang, X. Chen, J. Ma, S.C.J. Loo, W.D. Wei, Y. Yang, J.T. Hupp, F. Huo, Imparting functionality to a metal–organic framework material by controlled nanoparticle encapsulation, Nat. Chem. 4 (2012) 310–316, https://doi.org/10.1038/nchem.1272.
[50] X. Liu, L. He, J. Zheng, J. Guo, F. Bi, X. Ma, K. Zhao, Y. Liu, R. Song, Z. Tang, Solar-light-driven renewable butanol separation by core-shell Ag@ZIF-8 nanowires, Adv. Mater. 27 (2015) 3273–3277, https://doi.org/10.1002/adma.201405583.
[51] I.-K. Ding, J. Zhu, W. Cai, S.-J. Moon, N. Cai, P. Wang, S.M. Zakeeruddin, M. Grätzel, M.L. Brongersma, Y. Cui, M.D. McGehee, Plasmonic dye-sensitized solar cells, Adv. Energy Mater. 1 (2011) 52–57, https://doi.org/10.1002/aenm.201000041.
[52] L. Chu, Z. Qin, J. Yang, X. Li, Anatase TiO2 nanoparticles with exposed {001} facets for efficient dye-sensitized solar cells, Sci. Rep. 5 (2015) 12143, https://doi.org/10.1038/srep12143.
[53] M.S. Góes, E. Joanni, E.C. Muniz, R. Savu, T.R. Habeck, P.R. Bueno, F. Fabregat-Santiago, Impedance spectroscopy analysis of the effect of TiO2 blocking layers on the efficiency of dye sensitized solar cells, J. Phys. Chem. C 116 (2012) 12415–12421, https://doi.org/10.1021/jp301694r.
[54] S. Wooh, Y.-G. Lee, M.N. Tahir, D. Song, M. Meister, F. Laquai, W. Tremel, J. Bisquert, Y.S. Kang, K. Char, Plasmon-enhanced photocurrent in quasi-solid-state dye-sensitized solar cells by the inclusion of gold/silica core–shell nanoparticles in a TiO2 photoanode, J. Mater. Chem. A. 1 (2013) 12627, https://doi.org/10.1039/c3ta11712j.
[55] M. Sastry, K.S. Mayya, K. Bandyopadhyay, pH Dependent changes in the optical properties of carboxylic acid derivatized silver colloidal particles, Colloids Surfaces A Physicochem. Eng. Asp. 127 (1997) 221–228, https://doi.org/10.1016/S0927-7757(97)00087-3.
[56] J.M. Ashraf, M.A. Ansari, H.M. Khan, M.A. Alzohairy, I. Choi, Green synthesis of silver nanoparticles and characterization of their inhibitory effects on AGEs formation using biophysical techniques, Sci. Rep. 6 (2016) 20414, https://doi.org/10.1038/srep20414.
[57] S.T. Gentry, M.W. Bezpalko, Surface plasmon response for anisotropic silver particles with dimensions below the electrostatic limit, J. Phys. Chem. C 114 (2010) 6989–6993, https://doi.org/10.1021/jp1004902.
[58] A. Campion, P. Kambhampati, Surface-enhanced Raman scattering, Chem. Soc. Rev. 27 (1998) 241–250, https://doi.org/10.1039/a827241z.
[59] S.R. Emory, S. Nie, Near-field surface-enhanced Raman spectroscopy on single silver nanoparticles, Anal. Chem. 69 (1997) 2631–2635, https://doi.org/10.1021/AC9701647.
[60] S. Nie, S.R. Emory, Probing single molecules and single nanoparticles by surface-enhanced Raman scattering, Science 275 (1997) 1102–1106, https://doi.org/10.1126/science.275.5303.1102.
[61] T.A. Makhetha, S.C. Ray, R.M. Moutloali, Zeolitic imidazolate framework-8-encapsulated nanoparticle of Ag/Cu composites supported on graphene oxide: synthesis and antibacterial activity, ACS Omega 5 (2020) 9626–9640, https://doi.org/10.1021/acsomega.9b03215.
[62] H. Imahori, Y. Matsubara, H. Iijima, T. Umeyama, Y. Matano, S. Ito, M. Niemi, N. V. Tkachenko, H. Lemmetyinen, Effects of *meso* -diarylamino group of porphyrins as sensitizers in dye-sensitized solar cells on optical, electrochemical, and photovoltaic properties, J. Phys. Chem. C 114 (2010) 10656–10665, https://doi.org/10.1021/jp102486b.
[63] H. Imahori, N.V. Tkachenko, V. Vehmanen, K. Tamaki, H. Lemmetyinen, Y. Sakata, S. Fukuzumi, An extremely small reorganization energy of electron transfer in Porphyrin−Fullerene dyad, J. Phys. Chem. 105 (2001) 1750–1756, https://doi.org/10.1021/JP003207N.
[64] H. Imahori, A. Fujimoto, S. Kang, H. Hotta, K. Yoshida, T. Umeyama, Y. Matano, S. Isoda, M. Isosomppi, N.V. Tkachenko, H. Lemmetyinen, Host–guest interactions in the supramolecular incorporation of fullerenes into tailored holes on porphyrin-modified gold nanoparticles in molecular photovoltaics, Chem. Eur J. 11 (2005) 7265–7275, https://doi.org/10.1002/chem.200500610.
[65] H. Choi, W.T. Chen, P.V. Kamat, *Know thy nano neighbor* . Plasmonic *versus* electron charging effects of metal nanoparticles in dye-sensitized solar cells, ACS Nano 6 (2012) 4418–4427, https://doi.org/10.1021/nn301137r.
[66] A. Takai, P.V. Kamat, Capture, store, and discharge. Shuttling photogenerated electrons across TiO $_2$ –silver interface, ACS Nano 5 (2011) 7369–7376, https://doi.org/10.1021/nn202294b.
[67] M. Grätzel, Recent advances in sensitized mesoscopic solar cells, Acc. Chem. Res. 42 (2009) 1788–1798, https://doi.org/10.1021/ar900141y.
[68] X. Li, Q. Yu, C. Yu, Y. Huang, R. Li, J. Wang, F. Guo, Y. Zhang, S. Gao, L. Zhao, Zinc-doped SnO2 nanocrystals as photoanode materials for highly efficient dye-sensitized solar cells, J. Mater. Chem. A. 3 (2015) 8076–8082, https://doi.org/10.1039/c5ta01176k.
[69] Q. Yu, Y. Wang, Z. Yi, N. Zu, J. Zhang, M. Zhang, P. Wang, High-efficiency dye-sensitized solar cells: the influence of lithium ions on exciton dissociation, charge recombination, and surface states, ACS Nano 4 (2010) 6032–6038, https://doi.org/10.1021/nn101384e.
[70] C.-C. Chueh, C.-I. Chen, Y.-A. Su, H. Konnerth, Y.-J. Gu, C.-W. Kung, K.C.-W. Wu, Harnessing MOF materials in photovoltaic devices: recent advances, challenges, and perspectives, J. Mater. Chem. A. 7 (2019) 17079–17095, https://doi.org/10.1039/C9TA03595H.
[71] Y. Li, A. Pang, C. Wang, M. Wei, Metal–organic frameworks: promising materials for improving the open circuit voltage of dye-sensitized solar cells, J. Mater. Chem. 21 (2011) 17259, https://doi.org/10.1039/c1jm12754c.
[72] H.A. Lopez, A. Dhakshinamoorthy, B. Ferrer, P. Atienzar, M. Alvaro, H. Garcia, Photochemical response of commercial MOFs: Al $_2$ (BDC) $_3$ and its use as active material in photovoltaic devices, J. Phys. Chem. C 115 (2011) 22200–22206, https://doi.org/10.1021/jp206919m.
[73] C.H. Hendon, D. Tiana, A. Walsh, Conductive metal–organic frameworks and networks: fact or fantasy? Phys. Chem. Chem. Phys. 14 (2012) 13120, https://doi.org/10.1039/c2cp41099k.
[74] L. Sun, M.G. Campbell, M. Dincă, Electrically conductive porous metal-organic frameworks, Angew. Chem. Int. Ed. 55 (2016) 3566–3579, https://doi.org/10.1002/anie.201506219.